Ultrafast time-resolved 2D imaging of laser-driven fast electron transport in solid density matter using an x-ray free electron laser

H. Sawada[1, a)], T. Yabuuchi[2,3], N. Higashi[4,b)], T. Iwasaki[4], K. Kawasaki[4], Y. Maeda[4], T. Izumi[4], Y. Nakagawa[4], K. Shigemori[4], Y. Sakawa[4], C. B. Curry[5,6], M. Frost[5], N. Iwata[4], T. Ogitsu[7], K. Sueda[3], T. Togashi[2,3], S. H. Glenzer[5], A. J. Kemp[7], Y. Ping[7], and Y. Sentoku[4]

[1] *Department of Physics, University of Nevada, Reno, Nevada 89557, USA*
[2] *Japan Synchrotron Radiation Research Institute, Hyogo 679-5198, Japan*
[3] *RIKEN SPring-8 Center, Hyogo 679-5148, Japan*
[4] *Institute of Laser Engineering, Osaka University, Suita, 565-0871 Osaka, Japan*
[5] *SLAC National Accelerator Laboratory, Menlo Park, CA, 94025, USA*
[6] *Department of Electrical and Computer Engineering, University of Alberta, Edmonton, AB, T6G 1H9, Canada*
[7] *Lawrence Livermore National Laboratory, Livermore, CA, 94550, USA*

a) hsawada@unr.edu
b) current address: Faculty of Engineering, Hokkaido University, Sapporo, Hokkaido 060-8628, Japan

Abstract
High-power, short-pulse laser-driven fast electrons can rapidly heat and ionize a high-density target before it hydrodynamically expands. The transport of such electrons within a solid target has been studied using two-dimensional (2D) imaging of electron-induced Kα radiation. However, it is currently limited to no or picosecond scale temporal resolutions. Here we demonstrate femtosecond time-resolved 2D imaging of fast electron transport in a solid copper foil using the SACLA x-ray free electron laser (XFEL). An unfocused collimated x-ray beam produced transmission images with sub-micron and ~10 fs resolutions. The XFEL beam, tuned to its photon energy slightly above the Cu K-edge, enabled 2D imaging of transmission changes induced by electron isochoric heating. Time-resolved measurements obtained by varying the time delay between the x-ray probe and the optical laser show that the signature of the electron-heated region expands at ~25% of the speed of light in a picosecond duration. Time-integrated Cu Kα images support the electron energy and propagation distance observed with the transmission imaging. The x-ray near-edge transmission imaging with a tunable XFEL beam could be broadly applicable for imaging isochorically heated targets by laser-driven relativistic electrons, energetic protons, or an intense x-ray beam.

I. INTRODUCTION

A high-power short-pulse laser interacting with a solid target at a laser intensity greater than 10^{18} W/cm^2 produces a large, energetic (fast) electron current.[1] Such electrons play a central role in transferring the laser energy absorbed near the surface to the deep inside of the target. Understanding the electron transport mechanisms is critical for the efficient generation of ultrafast secondary sources such as energetic ions, terahertz radiation, x-ray, and gamma-ray radiation, as well as for the creation of warm and hot dense matter in isochoric (constant volume) heating[2,3,4].

The transport of laser-driven fast electrons in a solid or high-density target has been diagnosed using two-dimensional (2D) imaging of Kα radiation. The characteristic line emission is produced when an energetic electron knocks out the K-shell electron of background ions. Thus, the spatial distribution of Kα emissions is directly related to the trace of the electrons in the target. For such measurements, a monochromatic crystal imager[5,6,7] has been extensively used to record time-integrated Kα images of a solid metal target[8,9,10,11,12] or a fluorescence tracer embedded in a low-Z target[13,14,15]. In the context of fast electron transport studies, several groups have demonstrated ultrafast time-resolved 2D imaging, such as 2D fiber bundles coupled to a streak camera[16] with a few tens of ps resolution, a dilation x-ray imager[17] with a ~7 ps resolution, and a chirped optical rear surface probe[18] with a 100 fs resolution. However, measuring the fast electron propagation inside a high-density target at the near speed of light requires a hard x-ray pulse with a large probing area and a femtosecond scale temporal resolution.

Here we present a novel time-resolved 2D x-ray imaging setup to visualize laser-driven fast electrons propagating in a solid-density copper foil using femtosecond x-ray free electron laser (XFEL) pulses. An unfocused collimated x-ray beam, in conjunction with a high spatial resolution detector, produced x-ray transmission images of the foil with 10 fs and sub-micron resolutions. We identified electron target heating with this imaging capability by measuring transmission changes in a K-absorption edge spectrum. As reported in several experiments[19,20,21], isochoric target heating, here with fast electrons, causes shifting, smearing, or both of a near-edge absorption spectrum, increasing in transmission at photon energies slightly above the K-edge. By tuning the XFEL's photon energy to ~9.05 keV, ~50 eV above the Cu K-edge of 8.989 keV, we measured a region in the Cu foil with increased x-ray transmission as a signature of electron heating and its temporal evolution in a picosecond temporal scale for the first time. To assess the feasibility of the time-resolved x-ray transmission imaging, we present an analysis of the experimental transmission of cold Cu foils and a comparison of the results of the transmission images with time-integrated Kα images.

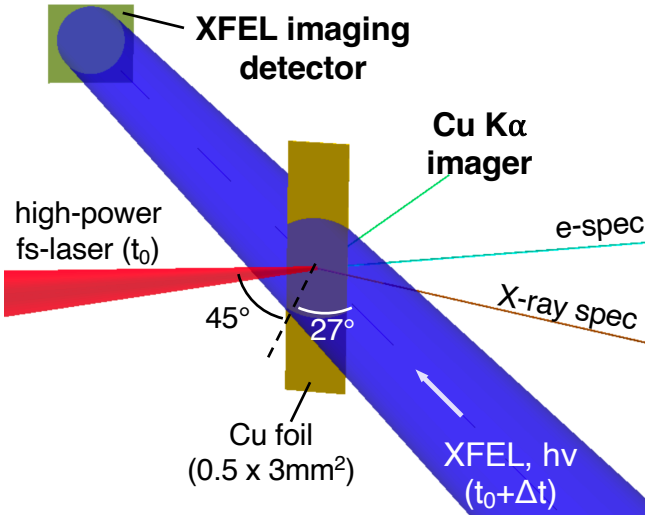

FIG. 1 A schematic diagram of the high-power laser-pump-XFEL probe experiment. An XFEL pulse transmitting through the Cu foil was recorded with a high spatial resolution detector using a CMOS camera. Laser-driven fast electrons and electron-induced Kα radiation were measured with a magnetic electron spectrometer (e-spec), a spherical crystal imager (Cu Kα imager) and a Bragg crystal spectrometer (X-ray spec).

II. EXPERIMENT

An XFEL experiment combined with a high-power short-pulse laser was carried out in the Experimental Hutch (EH) 6 of the SACLA beamline[22,23]. Figure 1 illustrates a schematic diagram of the experiment. A thin solid copper foil laser-cut into a 0.5×3 mm^2 size[24] was placed at the target chamber center. The foil thickness varied from 2, 10, and 25 μm. For the generation of a fast electron beam, the high-power femtosecond (fs) laser was focused on the foil with an f/10 parabola at an incident angle of 45°. The spot size and pulse duration were ~20 μm diameter and 40 fs at full width at half maximum (FWHM). A focused beam with a laser energy of 0.8 J resulted in a laser intensity of 1~2×10^{18} W/cm^2 at the best focus. According to the ponderomotive scaling[25], the electron energy distribution is predicted to have an exponential slope temperature of ~100 keV at this laser intensity. An unfocused 10-fs XFEL pulse probed the laser-irradiated foil with a 1 mm diameter spot at 27° from the target normal. As shown in the following sections, we varied the photon energy of the x-ray probe beam (hν) to obtain transmission of cold Cu foils in Sec. III A, and the time delay (Δt) of the x-ray beam with respect to the optical laser to measure the temporal evolution of fast electron transport in Sec. III B and III C.

Two primary diagnostics were x-ray transmission imaging with the XFEL pulses and Kα emission imaging based on a spherically bent crystal[5,6,7,26]. A single x-ray pulse transmitting through a cold or laser-irradiated foil was recorded with a 16-bit scintillator-based complementary metal-oxide-semiconductor (CMOS) image sensor. The camera had a pixel size of 6.5 μm square with 2048 × 2048 pixels (Hamamatsu Photonics ORCA-Flash4.0 v2)[27]. A magnification of 10 or 20 was chosen to probe the entire 500 μm width of the foil at the target plane. The effective pixel size was 0.3~0.6 μm, depending on the magnification in this experiment. Note that a higher optical magnification of up to 100 is available.[27] As briefly described in the introduction, the XFEL's tunability and narrow spectral bandwidth are essential for this technique using subtle changes in the K-absorption edge spectrum caused by target heating. The shape of an x-ray absorption edge of Fermi degenerate matter can be understood by a combination of the spectral resolution of measurements, the intrinsic broadening caused by the lifetime of the initial core state, and the temperature effect of the Fermi surface.[28,29] In a dense heated target with a temperature of > ~1 eV, the slope of an edge spectrum is predominantly

determined by the Fermi Dirac distribution function with a finite temperature representing the electron distribution near the Fermi surface.[30] For example, x-ray absorption near-edge spectroscopy in Ref.21 shows the smearing (broadening) of a Cu K-absorption edge in the range of a few tens of eV from the cold K-edge position. As a result, an x-ray transmission value slightly above the K-edge becomes higher than that of the cold sample. To ensure the x-ray beam's photon energy stays above the Cu K-edge of 8.989 keV, we set it to ~9.05 keV, larger than the spectral bandwidth of ~50 eV (FWHM), for x-ray transmission imaging in this experiment. As shown later in Figures 3 and 4, probing a laser-irradiated Cu foil at 9.05 keV shows a localized region where transmitted x-ray intensities increased. A quantitative estimate of the edge structure and transmission changes due to isochoric heating is an active research topic in high-energy-density science and is beyond this work's scope. Here, we focused on experimentally determining the temporal evolution of an electron-heated region by using near-edge transmission changes. The applicability and limitations of this technique based on the experiment are further discussed in Sec. III C.

The monochromatic x-ray imager for 8.05 keV Cu Kα consisted of a spherically bent quartz crystal, an x-ray CCD camera, and a beam block. The quartz crystal had a radius of curvature of 500 mm, the Miller indices of 21-31, and a Bragg angle of 88.7°. The distance from the laser interaction point to the crystal and from the crystal to the camera was 287 mm and 1947 mm, setting a magnification of 6.74. The effective pixel size was 3.0 μm/pixel with a camera's 20 μm pixel size (Princeton PIXIS-XB 1300B) and magnification. The spatial resolution was estimated to be ~8 μm from the sharpness of a grid image obtained in a separate experiment. The XFEL transmission imaging produced an instantaneous x-ray image at a delay of Δt after the optical laser irradiation, while the Cu Kα imaging was a time-integrated measurement. In addition, two secondary diagnostics were fielded to monitor shot-to-shot variations in fast electron generation: a magnetic electron spectrometer and a Bragg crystal spectrometer with a highly annealed pyrolytic graphite (HAPG)[31] crystal. The slope of a measured escaped electron spectrum provides information on the on-target laser intensity[32,33], while Cu Kα yields indicate the number of fast electrons colliding with the target. More details of the magnetic electron and x-ray spectrometer at EH6 are described elsewhere.[23] We recorded data on these four diagnostics on each shot at a rate of 3-5 minutes per shot.

III. EXPERIMENTAL RESUTS

A. Transmission measurements of cold Cu foils with the XFEL beam

We first recorded 2D x-ray images of cold Cu foils with the photon energy near the K-edge to demonstrate the method of measuring transmission with XFEL imaging. The tunability of the x-ray beam allowed us to

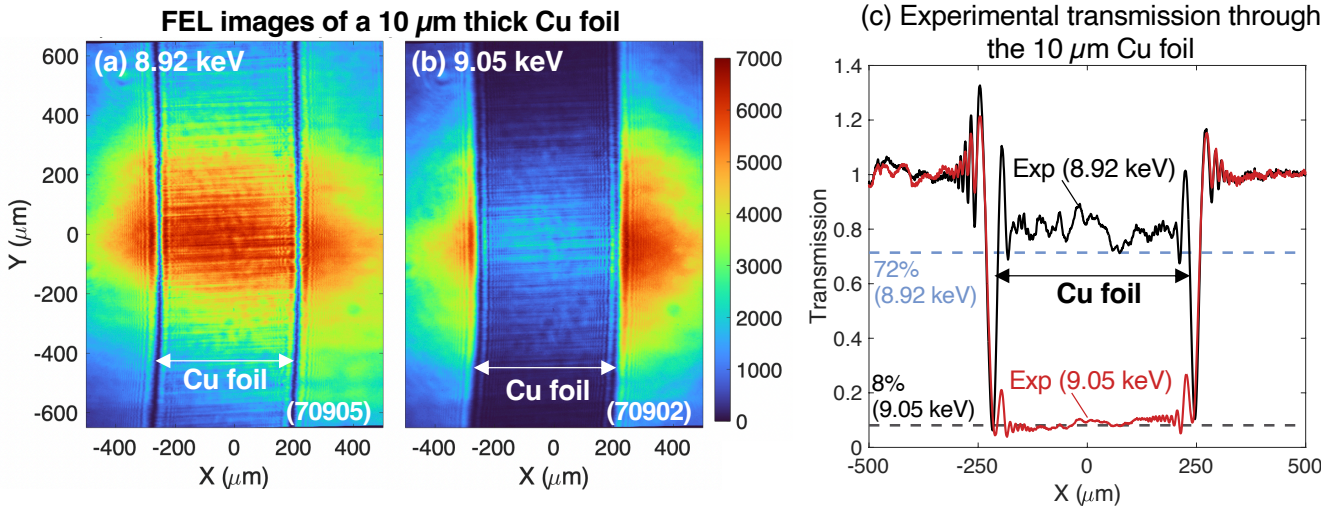

FIG.2 X-ray images of a 10 μm thick Cu foil at (a) 8.92 keV and (b) 9.05 keV. (c) Post-processed transmission profiles of the images shown in Fig.2(a) and 2(b). The reference profile was reconstructed by fitting the x-ray intensity distribution outside the foil with a polynomial function. The blue and black dashed lines in the figures are theoretical values.

measure a distinctive difference in 2D x-ray intensity maps below and above the K-edge. Figures 2(a) and 2(b) show x-ray images of a 10 μm thick Cu foil measured with the XFEL beam at 9.05 and 8.92 keV. The figures show that the x-ray intensity within the foil at 9.05 keV is significantly lower than that at 8.92 keV, as expected, due to the K-edge absorption. Here, we limited ourselves to using a 1D transmission profile because obtaining a 2D transmission image from consecutive shots with and without a target is difficult due to large spatial and intensity fluctuations of the XFEL pulse from the self-amplified spontaneous emission (SASE)[34]. Instead, a reference intensity profile [$I_0(x)$] was first reconstructed by fitting the measured profile [I(x)] outside of the foil for each shot. A 1D transmission profile was then calculated from a ratio of the two lineouts [$T(x) = I(x)/I_0(x)$]. Figure 2(c) shows 1D transmission profiles of the images in Figs. 2(a) and 2(b) together with the theoretical transmission values of a 10 μm thick Cu foil at 8.92 and 9.05 keV obtained from the tabulated transmission dataset[35] provided by the Center for X-ray Optics (CXRO). The spatially averaged transmission over the foil region is estimated to be 0.80 ± 0.10 and 0.09±0.09 at 8.92 keV and 9.05 keV, respectively. The error was estimated from the standard deviation of the measured transmission lineouts, the variation in transmission due to the XFEL's spectral bandwidth, and the transmission variation due to the foil thickness tolerance. The tolerance of the foil thickness is ±15% and ±25% for 25 μm and thinner ones (2 and 10 μm thick foils), respectively, according to the vendor (Goodfellow). In addition to the 10 μm thick foil measurements, we measured and systematically analyzed x-ray images of 2 and 25 μm thick Cu foils to obtain transmission. As summarized in Table 1, the experimental data reasonably agree with the theoretical values for the foil thicknesses and x-ray energies considered. This suggests that the analysis to obtain the 1D transmission profile using the reconstructed reference profile is adequate.

However, the measured 2D x-ray images and the transmission profiles of the cold Cu foils revealed several limitations in visualizing fast electron transport. (1) A thick sample foil, which strongly attenuates an x-ray probe intensity, particularly above the K-edge, could bury the experimental signature of a weak transmission signal into the background. For instance, the measured x-ray signal attenuated by the 25 μm thick Cu foil was only 20 counts above the background (~100 counts) at 9.05 keV. (2) Surface structures of a thick sample foil are more pronounced in an x-ray image than those of thin foils. As seen in Figs. 2(a) and 2(b), the grain on the surface of the 10 μm foil was imprinted in the x-ray images (photographs of Cu foils can be found in Ref.24). Any non-uniform structures such as the grain, foil defects, and/or scratches on the foil surfaces could interfere with a feature of transmission changes. In addition, a temperature gradient in the foil thickness direction must be carefully considered if a sample is thick. Considering these factors, we chose 2 μm thick foils as a test sample for visualizing fast electron transport in the foil, as shown in the next section.

Table 1 Summary of experimental and theoretical transmission with the two x-ray probe energies

	XFEL photon energy	T (Theory)	T (Exp)
2 μm Cu	8.924 keV	0.935	0.97±0.06
	9.051 keV	0.607	0.63±0.14
10 μm Cu	8.924 keV	0.716	0.80±0.10
	9.051 keV	0.082	0.09±0.09
25 μm Cu	8.924 keV	0.434	0.41±0.09
	9.051 keV	0.002	0.01±0.01

B. 2D transmission imaging of a high-power-laser-irradiated Cu foil

The 2D transmission image of a laser-irradiated Cu foil was obtained by analyzing two consecutive shots before and after high-power laser irradiation. Figures 3(a) and 3(b) show raw x-ray images of the two shots recorded with a camera magnification of 20. The x-ray photon energy was fixed to 9.05 keV. The reference image with the XFEL beam (run71387) allowed us to inspect the initial foil condition (density and thickness). In addition, it recorded diffraction fringes produced by the foil edges and defects in the foil, if any. The x-ray beam then imaged the same target irradiated by the optical laser at a time delay of Δt (0.7 ps for run71388). Although a slight increase in the x-ray intensity near the center is seen in Fig. 3(b), it is difficult to quantitatively evaluate the spatial size of the electron-heated region in the raw image. Instead, dividing the two images cancels out most diffraction fringe patterns, making the transmission change's contrast more apparent. In Figure 3(c), the result of the image division shows a somewhat circular enhanced transmission region. The size of the experimental feature expands with time, as shown in the next section. In Fig.3(c) and most shots, a strong

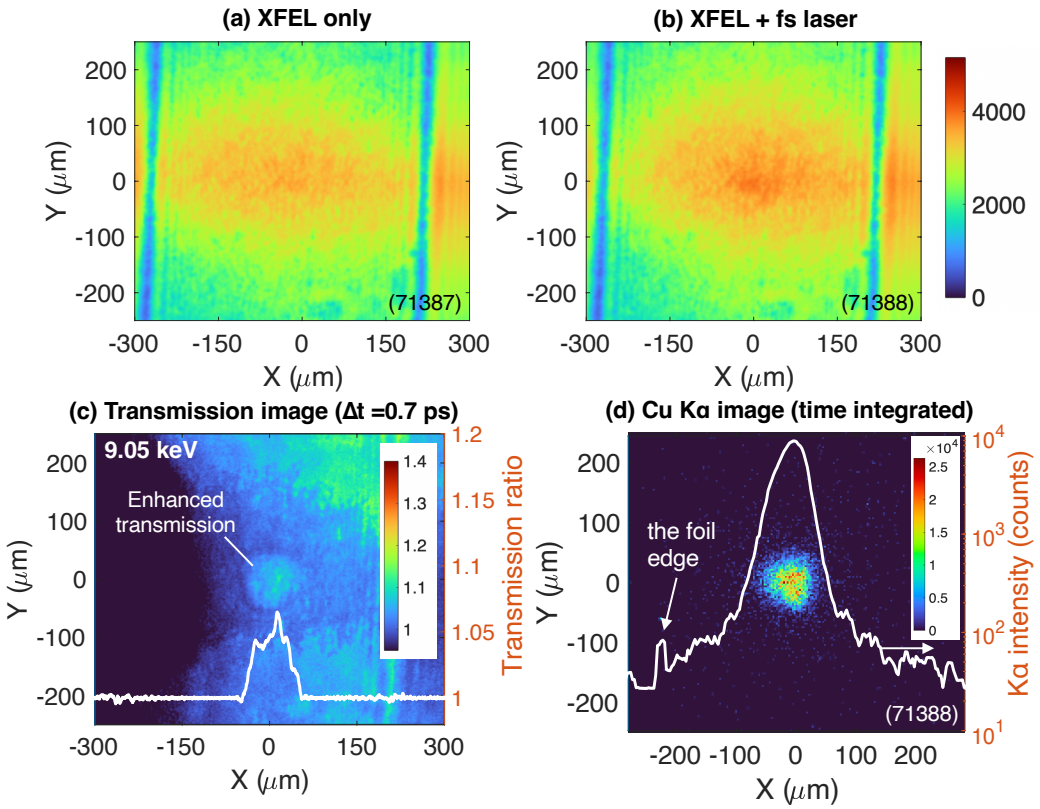

FIG.3 Raw x-ray images of a 2 μm thick Cu foil (a) before and (b) after the optical laser irradiation at 0.7 ps. (c) Result of the image division of (b) by (a). The solid white line shows a horizontal lineout of the normalized transmission. (d) Cu Kα image for run 71388 and a lineout of the emission spot along the x-axis on the log scale.

gradient in transmission remains across the resulting image even after the image division due to the stochastic nature of the SASE XFEL beam. Therefore, it was further processed to remove the gradient by applying a masking function outside the region of interest. A horizontal lineout of the normalized transmission image to the unity is superposed in Fig. 3(c). A series of transmission images recorded at various time delays are presented and discussed in the next section.

Time-integrated Cu Kα imaging provided additional information on the laser-driven fast electrons to support the results of the XFEL transmission imaging. Figure 3(d) shows a Kα image in the same target shot shown in Fig. 3(b) (run71388). The spatial extent of the Kα emission can be correlated to the collisional stopping distance of energetic electrons in a solid-density target.[36] A Gaussian profile fitting to the central peak of the lineout yielded 54.2 μm in FWHM, corresponding to the mean energy of an electron spectrum of ~100 keV according to the continuous-slowing-down approximation (CSDA) distance[37]. The electron energy estimated is consistent with the ponderomotive scaling at the laser intensity used in this experiment. Fig. 3(d) also shows the emission signals produced at the foil edge, indicating the generation of high-energy electrons (> ~0.5 MeV) whose CSDA distance is ~250 μm, although the number of the electrons is approximately two orders of magnitude smaller than the ones producing the central Kα peak. Lineouts of the time-integrated Kα emission spots and time-resolved transmission images are compared in the next section.

C. Time-resolved measurements of fast electron transport in a solid Cu foil

The temporal evolution of fast electron propagation identified as increased transmission signals was measured by delaying the x-ray probe timing. Figure 4 shows lineouts of the transmission spot observed at a time delay of 0.2 ps, 0.7 ps, and 1.2 ps and compares them with those of the Kα emission spot for the corresponding shots. The size (width) of the enhanced transmission region is evaluated by taking the horizontal lineout averaged over the spatial resolution and using a threshold based on 5% of the averaged signal near the

peak of a transmission ratio. Here, we used horizontal lineouts instead of azimuthally averaged profiles because the shape of an enhanced transmission region is not necessarily round due to the incident angle of the laser and the x-ray beam. After considering these view angles, the measurements show that the width of the electron-heated region was 64.1 μm, 95.8 μm, and 133.2 μm at 0.2, 0.7, and 1.2 ps, respectively. The expansion of the heated area was no longer observed after ~1.2 ps. The spatial and temporal uncertainties of the measurements were ±2.9 μm and ±0.1 ps. Therefore, the speed of the expanding electron heat front is estimated to be 63.4±19.1 μm/ps (0.21c±0.06c) from 0.2 ps to 0.7 ps and 74.8±23.1 μm/ps (0.25c±0.08c) from 0.7 ps to 1.2 ps, where c is the speed of light. Since the timing jitter and spatial resolution were 0.1 ps and ~3 μm in the current setup, this technique can capture an electron heat front propagating at the speed of light (i.e., 300 μm/ps).

On the other hand, the Kα profiles, fitted with a Gaussian function, yielded the FWHM of 47.1, 54.2, and 58.9 μm for these three shots. The average FWHM and the standard deviation over 38 shots were 58.3 ± 5.2 μm. The fluctuation is likely due to target positioning and manual target mounting variations. Nonetheless, the size of the measured Kα emission spots is comparable to the stopping distance of ~ 100 keV electrons. The x-ray transmission and Kα image measurements suggest that fast electron isochoric heating of a solid Cu at the laser intensity we used is driven by ~100 keV electrons rather than the much smaller number of sub-MeV electrons.

The XFEL-based transmission imaging presented here could be a versatile diagnostic for various thicknesses and materials of targets in isochoric heating with a variety of heating sources. As shown in Fig.4, the transmission ratio increased by 3~6% after heating, and the signal-to-noise ratio was 12~20 in our measurements. With the threshold of 5% of the peak signal, this technique could be applied to measuring a transmission change in a minimum of ~150 nm Cu foil at 9.05 keV, provided that the density and thickness remain constant during the heating. Furthermore, the XFEL's wavelength tunability provides great flexibility in selecting a target material to be studied using either a K- or L-absorption edge. Changes in the near-edge absorption spectrum have been observed with various pump drivers, including laser-driven relativistic electrons[21], energetic protons[19], an XFEL beam[20], a non-relativistic intensity laser[38], and current-driven magnetic cylindrical compression[39,40]. In our experiment at a relativistic laser intensity of ~10^{18} W/cm^2, we measured

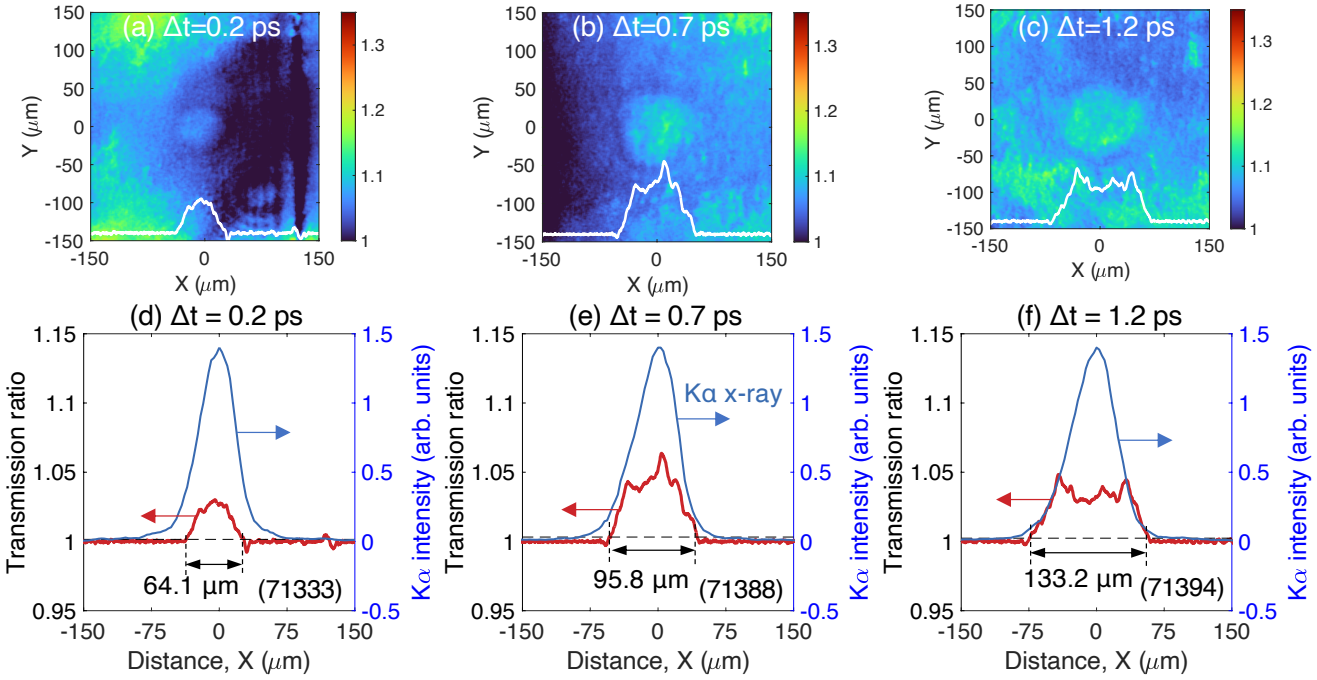

FIG.4 Experimental transmission images at (a) 0.2 ps, (b) 0.7 ps, and (c) 1.2 ps. Comparisons of lineouts of the increased transmission regions (red) with those of time-integrated Cu Kα emission spots (blue) at a time delay of (d) 0.2 ps, (e) 0.7 ps, and (f) 1.2 ps. The horizontal dashed line indicates the error level estimated from 5% of the averaged signal near the peak in the transmission image on each shot.

an increase in x-ray transmission at a photon energy of 50 eV above the K-edge but not ~140 eV (at 9.12 keV), while a transmission decrease was observed at ~60 eV below the K-edge (at 8.92 keV), indicating the smearing of the near-edge spectrum occurred due to the fast electron heating.[41] Diagnosing the plasma condition from the modified Cu K-edge transmission spectrum will be reported in a future publication.

IV. SUMMARY

We have demonstrated an XFEL-based time-resolved 2D imaging diagnostic to measure laser-driven fast electron transport in a solid Cu foil. The 10-fs x-ray probe pulse with the photon energy slightly above the Cu K-edge visualized an increased transmission spot as a signature of fast electron isochoric heating of the foil. The time-resolved transmission measurements show that the electron-driven heat front propagated at approximately a quarter of the speed of light in a picosecond. The time-integrated Kα emission images confirm the mean energy of the fast electrons and the electron propagation distance observed in the transmission measurements. The x-ray transmission imaging presented could be a spatiotemporally resolved powerful diagnostic to probe the condition of an isochorically heated high-density target by ultrafast heating sources such as relativistic electrons, energetic protons, or a direct x-ray beam.

ACKNOWLEDGEMENTS

The XFEL experiments were performed at the BL2 of SACLA with the approval of the Japan Synchrotron Radiation Research Institute (JASRI) (Proposal No. 2019A8002). This material is based on the work supported by the National Science Foundation under Grant No. 1707357 and 2010502 through the NSF/DOE Partnership in Basic Plasma Science and Engineering. Y.S. and N.I. are supported by JSPS Kakenhi Grants No. JP20H00140, 20K14439 and JP19KK0072. T.I., K.K., Y.M., and K. Shigemori are supported by JSPS Kakenhi Grants No.17H02996. The work of T.O, A.J.K., and Y.P. was supported by the U.S. Department of Energy by the Lawrence Livermore National Laboratory under Contract No. DE-AC52-07NA27344 and funded by the DOE Office of Science Early Career Program under SCW 1265 (A.J.K.) and SCW 1420 (Y.P.). The work of C.B.C., M.F., and S.H.G was supported by the U.S. Department of Energy (DOE), Office of Science, Fusion Energy Sciences under FWP 100182. C.B.C was also partially supported by the Natural Sciences and Engineering Research Council of Canada (NSERC). T. I., Y. N., and Y. Sakawa were supported by JSPS Kakenhi Grants No.17H06202 and JSPS Core-to-Core Program B: Asia-Africa Science Plat-forms Grant No. JPJSCCB20190003.

AUTHOR DECLARATIONS

Conflict of Interest

The authors have no conflicts to disclose.

DATA AVAILABILITY

The data that support the findings of this study are available from the corresponding author upon reasonable request.

[1] P. Gibbon, Short Pulse Laser Interactions with Matter: An Introduction (Imperial College Press, London, 2005)
[2] Z. Jiang, J. C. Kieffer, J. P. Matte, M. Chaker, O. Peyrusse, D. Gilles, G. Korn, A. Maksimchuk, S. Coe, and G. Mourou, Phys. Plasmas 2, 1702 (1995).
[3] J. Workman, A. Maksimchuk, X. Liu, U. Ellenberger, J. S. Coe, C.-Y. Chien, and D. Umstadter, Phys. Rev. Lett. 75, 2324 (1995).
[4] A. Saemann, K. Eidmann, I. E. Golovkin, R. C. Mancini, E. Andersson, E. Förster, and K. Witte, Phys. Rev. Lett. 82, 4843 (1999).
[5] Y. Aglitskiy, T. Lehecka, S. Obenschain, C. Pawley, C. M. Brown, and J. Seely, Rev. Sci. Instrum. 70, 530 (1999)
[6] J.A. Koch, Y. Aglitskiy, C. Brown, T. Cowan, R. Freeman, S. Hatchett, G. Holland, M. Key, A. MacKinnon, J. Seely, R. Snavely, and R. Stephens, Rev. Sci. Instrum. 74, 2130 (2003).
[7] M.S. Schollmeier and G.P. Loisel, Rev. Sci. Instrum. 87, 123511 (2016).
[8] D.C. Eder, G. Pretzler, E. Fill, K. Eidmann, and A. Saemann, Appl. Phys. B 2000 702 70, 211 (2000).
[9] K.U. Akli, M.H. Key, H.K. Chung, S.B. Hansen, R.R. Freeman, M.H. Chen, G. Gregori, S. Hatchett, D. Hey, N. Izumi, J. King, J. Kuba, P. Norreys, a. J. Mackinnon, C.D. Murphy, R. Snavely, R.B. Stephens, C. Stoeckel, W. Theobald, and B. Zhang, Phys. Plasmas 14, 023102 (2007).
[10] V.M. Ovchinnikov, G.E. Kemp, D.W. Schumacher, R.R. Freeman, and L.D. Van Woerkom, Phys. Plasmas 18, 072704 (2011).
[11] T. Ma, H. Sawada, P.K. Patel, C.D. Chen, L. Divol, D.P. Higginson, A. J. Kemp, M.H. Key, D.J. Larson, S. Le Pape, A. Link, A. G. MacPhee, H.S. McLean, Y. Ping, R.B. Stephens, S.C. Wilks, and F.N. Beg, Phys. Rev. Lett. 108, 115004 (2012).
[12] H. Sawada, Y. Sentoku, T. Yabuuchi, U. Zastrau, E. Förster, F.N. Beg, H. Chen, A.J. Kemp, H.S. McLean, P.K. Patel, and Y. Ping, Phys. Rev. Lett. 122, 155002 (2019).

[13] K.B. Wharton, S.P. Hatchett, S.C. Wilks, M.H. Key, J.D. Moody, V. Yanovsky, A.A. Offenberger, B.A. Hammel, M.D. Perry, and C. Joshi, Phys. Rev. Lett. 81, 822 (1998).
[14] R. Stephens, R. Snavely, Y. Aglitskiy, F. Amiranoff, C. Andersen, D. Batani, S. Baton, T. Cowan, R. Freeman, T. Hall, S. Hatchett, J. Hill, M. Key, J. King, J. Koch, M. Koenig, a. MacKinnon, K. Lancaster, E. Martinolli, P. Norreys, E. Perelli-Cippo, M. Rabec Le Gloahec, C. Rousseaux, J. Santos, and F. Scianitti, Phys. Rev. E 69, 066414 (2004).
[15] L.C. Jarrott, M.S. Wei, C. McGuffey, A.A. Solodov, W. Theobald, B. Qiao, C. Stoeckl, R. Betti, H. Chen, J. Delettrez, T. Döppner, E.M. Giraldez, V.Y. Glebov, H. Habara, T. Iwawaki, M.H. Key, R.W. Luo, F.J. Marshall, H.S. McLean, C. Mileham, P.K. Patel, J.J. Santos, H. Sawada, R.B. Stephens, T. Yabuuchi, and F.N. Beg, Nat. Phys. 12, 499 (2016).
[16] R. Kodama, K. Okada, and Y. Kato, Rev. Sci. Instrum. 70, 625 (1999).
[17] S.R. Nagel, H. Chen, J. Park, M. Foord, A.U. Hazi, T.J. Hilsabeck, S.M. Kerr, E. V. Marley, and G.J. Williams, Appl. Phys. Lett. 110, 144102 (2017).
[18] J.S. Green, N. Booth, R.J. Dance, R.J. Gray, D.A. MacLellan, A. Marshall, P. McKenna, C.D. Murphy, C.P. Ridgers, A.P.L. Robinson, D. Rusby, R.H.H. Scott, and L. Wilson, Sci. Rep. 8, 4525 (2018).
[19] A. Mančić, A. Lévy, M. Harmand, M. Nakatsutsumi, P. Antici, P. Audebert, P. Combis, S. Fourmaux, S. Mazevet, O. Peyrusse, V. Recoules, P. Renaudin, J. Robiche, F. Dorchies, and J. Fuchs, Phys. Rev. Lett. 104, 1 (2010).
[20] D.S. Rackstraw, O. Ciricosta, S.M. Vinko, B. Barbrel, T. Burian, J. Chalupský, B.I. Cho, H.-K. Chung, G.L. Dakovski, K. Engelhorn, V. Hájková, P. Heimann, M. Holmes, L. Juha, J. Krzywinski, R.W. Lee, S. Toleikis, J.J. Turner, U. Zastrau, and J.S. Wark, Phys. Rev. Lett. 114, 015003 (2015).
[21] Y. Inubushi, T. Yabuuchi, K. Miyanishi, K. Sueda, T. Togashi, Y. Kubota, K. Tono, and M. Yabashi, Rev. Sci. Instrum. 92, 053534 (2021).
[22] K. Tono, T. Togashi, Y. Inubushi, T. Sato, T. Katayama, K. Ogawa, H. Ohashi, H. Kimura, S. Takahashi, K. Takeshita, H. Tomizawa, S. Goto, T. Ishikawa, and M. Yabashi, New J. Phys. 15, 083035 (2013).
[23] T. Yabuuchi, A. Kon, Y. Inubushi, T. Togahi, K. Sueda, T. Itoga, K. Nakajima, H. Habara, R. Kodama, H. Tomizawa, and M. Yabashi, J. Synchrotron Radiat. 26, 585 (2019).
[24] M. Frost, C.B. Curry, and S.H. Glenzer, J. Instrum. 15, P05004 (2020).
[25] S. C. Wilks, W. L. Kruer, M. Tabak, and A. B. Langdon, Phys. Rev. Lett. 69, 1383 (1992).
[26] H. Sawada, T. Daykin, H.S. McLean, H. Chen, P.K. Patel, Y. Ping, and F. Pérez, Rev. Sci. Instrum. 88, 063502 (2017).
[27] T. Kameshima, A. Takeuchi, K. Uesugi, T. Kudo, Y. Kohmura, K. Tamasaku, K. Muramatsu, T. Yanagitani, M. Yabashi, and T. Hatsui, Opt. Lett. **44**, 1403 (2019).
[28] C. F. Hague, Phys. Rev. B 25, 3529 (1982).
[29] K. Oguri, Y. Okano, T. Nishikawa, and H. Nakano, Phys. Rev. Lett. 99, 165003 (2007).
[30] F. Dorchies, F. Festa, V. Recoules, O. Peyrusse, A. Benuzzi-Mounaix, E. Brambrink, A. Levy, A. Ravasio, M. Koenig, T. Hall, and S. Mazevet, Phys. Rev. B 92, 085117 (2015).
[31] U. Zastrau, A. Woldegeorgis, E. Förster, R. Loetzsch, H. Marschner, and I. Uschmann, J. Instrum. 8, P10006 (2013).
[32] A. Link, R. R. Freeman, D. W. Schumacher, and L. D. Van Woerkom, Phys. Plasmas 18, 053107 (2011).
[33] L. Chen and H. Sawada, Phys. Plasmas 29, 93104 (2022).
[34] R. Bonifacio, C. Pellegrini, and L. M. Narducci, Opt. Commun. 50, 373–378 (1984).
[35] B.L. Henke, E.M. Gullikson, and J.C. Davis, At. Data Nucl. Data Tables 54, 181 (1993) and the website: https://henke.lbl.gov/optical_constants/
[36] H. Sawada, J. Trzaska, C.B. Curry, M. Gauthier, L.B. Fletcher, S. Jiang, H.J. Lee, E.C. Galtier, E. Cunningham, G. Dyer, T.S. Daykin, L. Chen, C. Salinas, G.D. Glenn, M. Frost, S.H. Glenzer, Y. Ping, A.J. Kemp, and Y. Sentoku, Rev. Sci. Instrum. 92, 13510 (2021).
[37] M. J. Berger, "ESTAR, PSTAR and ASTAR: Computer programs for calculating stopping-power and range tables for electrons, protons and helium ions," Report No. NISTIR 4999, National Institute of Standards and Technology, Gaithersburg, 1992.
[38] B.I. Cho, K. Engelhorn, A.A. Correa, T. Ogitsu, C.P. Weber, H.J. Lee, J. Feng, P.A. Ni, Y. Ping, A.J. Nelson, D. Prendergast, R.W. Lee, R.W. Falcone, and P.A. Heimann, Phys. Rev. Lett. 106, 167601 (2011).
[39] S.B. Hansen, E.C. Harding, P.F. Knapp, M.R. Gomez, T. Nagayama, and J.E. Bailey, High Energy Density Phys. 24, 39 (2017).
[40] S.B. Hansen, E.C. Harding, P.F. Knapp, M.R. Gomez, T. Nagayama, and J.E. Bailey, Phys. Plasmas 25, 056301 (2018).
[41] H. Sawada et al., 64th Annual Meeting of the APS Division of Plasma Physics, Abstract: CI01.00003: Femtosecond dynamics of relativistic electron heating in a high-intensity laser-produced solid-density plasma, (2022). https://meetings.aps.org/Meeting/DPP22/Session/CI01.3